EPJ Web of Conferences **259**, 01004 (2022) https://doi.org/10.1051/epjconf/202225901004
SQM 2021

Heavy ion results from LHCb

Jiayin Sun (for the LHCb collaboration)[1,2,*]

[1]Università degli Studi di Cagliari, Cagliari, Italy
[2]INFN Sezione di Cagliari, Cagliari, Italy

Abstract. The LHCb detector is a single-arm spectrometer fully instrumented in the forward rapidity at the LHC. In this contribution we introduce some of the most recent results in heavy ion collisions, the upgrades for LHC Run3 and the future perspectives of the heavy ion program from the LHCb experiment.

1 Introduction

The LHCb detector [1] is a single-arm forward spectrometer fully instrumented in the pseudorapidity range $2 < \eta < 5$. The detector includes a high-precision tracking system providing excellent vertex and momentum resolution, two ring-imaging Cherenkov detectors for charged particle identification, a calorimeter system to identify photons, electrons and hadrons, and a muon system. The coverage in the forward rapidity region is complementary to other major experiments at the LHC, and allows unique access to Bjorken-x region $\sim 10^{-6} - 1$[2–4] inside the nucleus. With the introduction of the SMOG (System for Measuring overlap with gas) in 2015, the LHCb detector is equipped with the unique capability to operate in fixed-target configuration and study beam-gas collisions at lower energies using noble gas targets injected inside the primary LHC vacuum.

LHCb has collected a variety of heavy-ion data in recent years. In the standard beam-beam collision mode, pPb and Pbp collisions are recorded at $\sqrt{s_{\rm NN}} = 5.02$ TeV with a total luminosity of ~ 1.6 nb^{-1} in year 2013, and at $\sqrt{s_{\rm NN}} = 8.16$ TeV with a total luminosity around 35 nb^{-1} in 2016. PbPb collisions at $\sqrt{s_{\rm NN}} = 5.02$ TeV are also collected in 2015 and 2018 with a luminosity of $\sim 10\,\mu$b^{-1} and $210\,\mu$b^{-1}, respectively.

2 Recent heavy-ion results

2.1 Prompt charged hadron production in pp and pPb collisions at 5.02 TeV

The production of prompt charged hadrons is measured with precision in pp and pPb collisions at 5.02 TeV [5]. Since the LHCb detector covers only one direction in rapidity, two beam configures of pPb collisions are used. In the pPb or forward configuration, the proton beam travels from the vertex detector VELO to the muon chambers. In the Pbp or backward configuration, the directions of the proton and lead beams are switched. The double-differential cross-section of prompt charged hadrons as a function of transverse momentum, $p_{\rm T}$, in the range of $0.2 < p_{\rm T} < 8$ GeV/c, is shown in Fig. 1. The pseudorapiditiy (η) acceptance

*e-mail: jiayin.sun@cern.ch

covers $2.0 < \eta < 4.8$ for pp, $1.5 < \eta < 4.3$ for pPb and $-5.2 < \eta < -2.5$ for Pbp, and is divided into 6 η bins in this measurement. The prompt charged hadrons are measured with the LHCb tracking system. Their yields are corrected for the reconstruction and selection efficiency, as well as contamination from ghost tracks and non-prompt particles. The total uncertainty of the production cross-section is about 3% for most (p_{T}, η) bins.

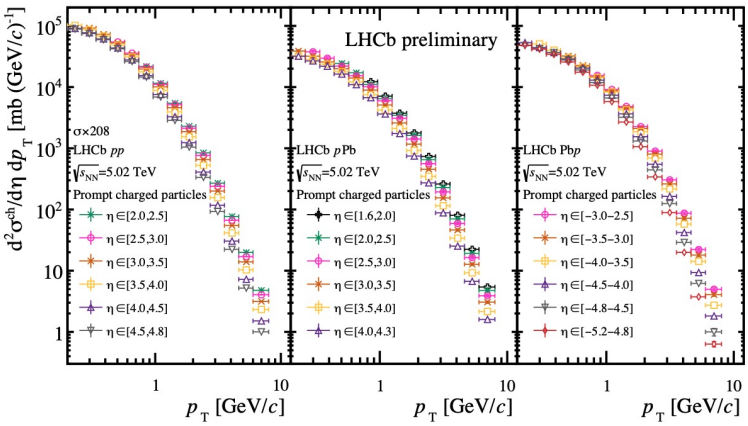

Figure 1. Double differential cross-section of prompt charged hadron production in pp (left), pPb (middle) and Pbp (right) collisions at $\sqrt{s_{\mathrm{NN}}} = 5.02$ TeV.

The nuclear modification factor $R_{p\mathrm{Pb}}$ is presented in Fig. 2. The five upper (lower) panels show $R_{p\mathrm{Pb}}$ as a function of p_{T} in the pPb (Pbp) configuration. A significant suppression is observed in the forward region. The $R_{p\mathrm{Pb}}$ value reaches ~ 0.3 at lowest p_{T} in the most forward pseudorapidity bin. In the backward region, an enhancement is found for $p_{\mathrm{T}} > 1.5$ GeV/c. The measurement is compared to calculations from three phenomenological models in the region $p_{\mathrm{T}} \geq 1.5$ GeV/c. The calculation using nuclear PDFs [6] agrees with the forward data within large nPDF uncertainties, but does not reproduce the enhancement in the backward region. The gluon saturation model [7] qualitatively describes the increasing trend in the forward rapidity. In the backward rapidity, the data are not well described by the pQCD calculation considering parton multiple scattering [8].

2.2 Prompt production ratio of χ_{c2}/χ_{c1} in pPb collisions at 8.16 TeV

The χ_{c2} and χ_{c1} charmonium production in nuclear collisions at LHC energies is first measured by the LHCb with pPb collisions at 8.16 TeV [9]. The χ_{cJ} states are reconstructed via the decay $\chi_c \to J/\psi(\to \mu^+\mu^-)\gamma$ The J/ψ candidates are reconstructed from a pair of oppositely charged muons. They are combined with a photon candidate to form a χ_c candidate. Two types of photons are used in this analysis: photons converted into electron positron pairs in the detector material and reconstructed by the tracking system (*converted photons*), and photons from their energy deposits in the electromagnetic calorimeter (*calorimetric photons*). The χ_{c1} and χ_{c2} signals reconstructed via converted photons are shown in the left panel of Fig. 3, while those reconstructed via calorimetric photons are shown in the right. The converted photon technique provides better mass resolution with well separated χ_{c1} and χ_{c2} peaks, whereas the calorimetric photon technique provides ~ 20 times more statistics. An upper limit of the pseudo-decay time, $t_z < 0.1$ ps, is imposed to remove non-prompt χ_c production from b-hadron decays.

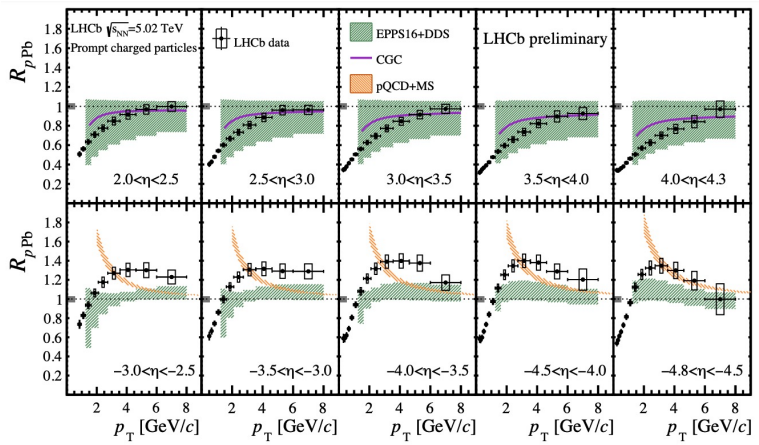

Figure 2. The nuclear modification factor $R_{p\mathrm{Pb}}$ of prompt charged hadrons as a function of p_T in the forward (upper) and backward (lower) rapidity regions.

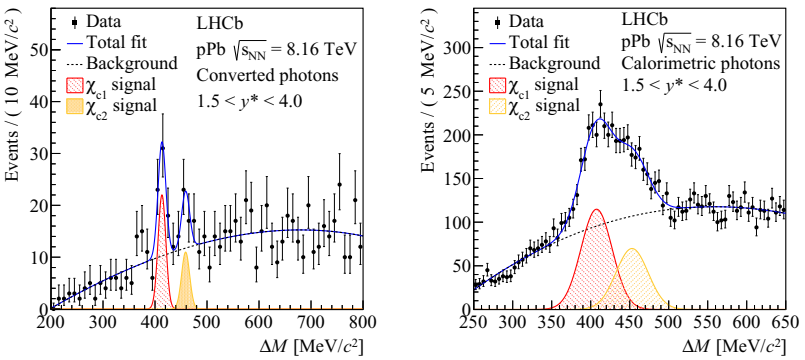

Figure 3. Invariant mass distribution of χ_{c1} and χ_{c2} candidates in pPb collisions reconstructed via the converted photon method (left) and via the calorimetric photon method (right).

As the χ_{c1} and χ_{c2} decays share nearly identical kinematics, various detector effects in the ratio of $\sigma\chi_{c2}/\sigma\chi_{c1}$, such as tracking and particle identification efficiencies, are cancelled, reducing the systematic uncertainty of the measurement. The measured ratio is presented in Fig. 4. The $\sigma\chi_{c2}/\sigma\chi_{c1}$ ratios measured with the two photon types are consistent with each other, and with unity in both the forward and backward rapidity regions. The significantly larger calorimetric photon sample allows for a more precise measurement. The cross-section ratio in pPb data is also compared with a similar measurement from pp collisions at $\sqrt{s} = 7$ TeV [10]. The results are consistent within two standard deviations. This implies that nuclear effects, if any, have the similar impacts on both states.

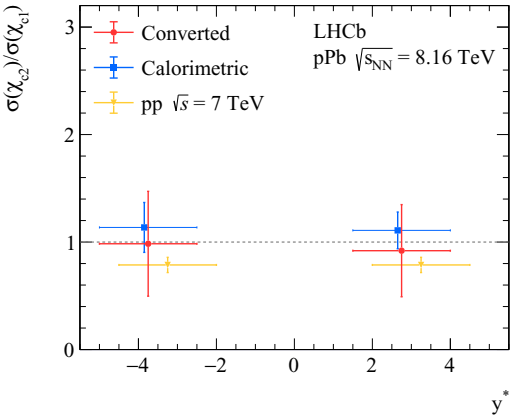

Figure 4. Production cross-section ratio $\sigma\chi_{c2}/\sigma\chi_{c1}$ measured in the forward and backward rapidity regions. The error bars reflect the total uncertainties.

2.3 Coherent J/ψ production in peripheral PbPb collisions at $\sqrt{s_{\rm NN}}$ = 5.02 TeV

One of the first results of AA collisions from LHCb, the photo-production of J/ψ at low transverse momentum is studied in peripheral lead-lead collisions at $\sqrt{s_{\rm NN}} = 5.02$ TeV, using a data sample collected by LHCb in 2018 with an integrated luminosity of 210 μb^{-1} [11]. The J/ψ meson candidates are reconstructed through the $J/\psi \to \mu^+\mu^-$ decay channel. The dimuon invariant mass distribution of the selected candidates is shown in the left of Fig. 5 for J/ψ candidates with $p_{\rm T} < 15.0\,{\rm GeV}/c$ and $2.0 < y < 4.5$ in a peripheral centrality interval corresponding to $\langle N_{part}\rangle = 10.6 \pm 2.9$. The prompt J/ψ candidates are selected using the requirement on the pseudo decay-time $t_z < 0.3$ ps. The photo-produced J/ψ mesons and the hadronically produced J/ψ mesons are separated with an unbinned maximum likelihood fit to the dimuon $ln(p_{\rm T}^2)$ spectrum, as shown in the right of Fig. 5. The photo-produced J/ψ candidates (red dotted line) are visible in the range $0 < p_{\rm T} < 250\,{\rm MeV}/c$.

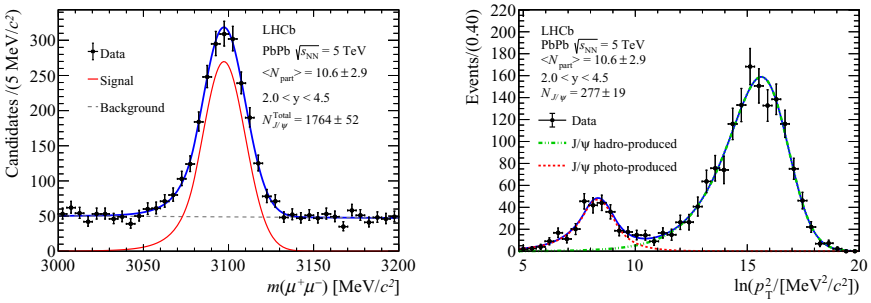

Figure 5. Left: invariant mass distribution of J/ψ candidates in $p_{\rm T} < 15.0\,{\rm GeV}/c$ and $2.0 < y < 4.5$, with $\langle N_{part}\rangle = 10.6 \pm 2.9$. Right: the $lnp_{\rm T}^2$ distribution of J/ψ candidates after background subtraction for the same kinematic interval.

Figure 6 presents the measured production yield of photo-produced J/ψ mesons as a function of $p_{\rm T}$ (left), and rapidity, y, (right), determined for the first time at the LHC. The mean

p_T of the coherent J/ψ is estimated to be $\langle p_T \rangle = 64.9 \pm 2.4$ MeV/c. Theoretical calculations [12, 13] are drawn in open circles, and are qualitatively in agreement with the data in the p_T and y shape.

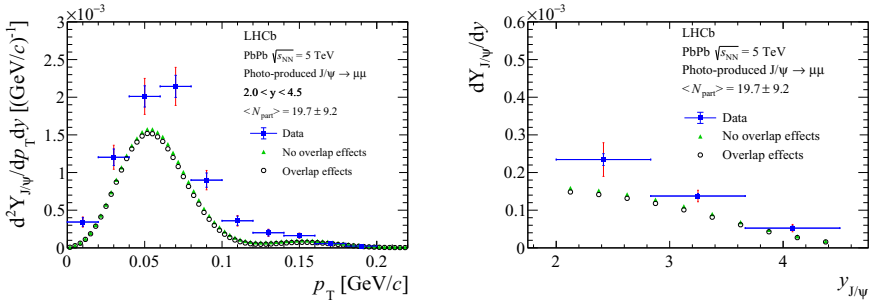

Figure 6. Invariant yields of photo-produced J/ψ mesons as a function of p_T (left) and rapidity (right), for the centrality interval $\langle N_{part} \rangle = 19.7 \pm 9.2$. The blue error bars represent the statistical uncertainty and the red error bars the total uncertainty. Theoretical model predictions [12, 13] are shown in open circles in black and green.

3 Upgrade and future plans

During the LHC Long Shutdown 2 the LHCb is undergoing a major upgrade [14] to meet the challenge of the increased luminosity in the LHC Run3. A new software-only trigger system with 40 MHz data acquisition and real time data reconstruction will replace the current trigger system using a hardware-based trigger step. The detector readout scheme is being upgraded to allow event processing at 40 MHz rate. Upgrades of the sub-detectors include a new Vertex Locator (VELO) with pixel segmentation, new tracking stations and new RICH optics and PMTs. The upgrade will reduce the occupancy limitation in PbPb collisions, and allow access to mid-central PbPb collisions up to 30% in centrality.

The upgrade of the LHCb's fixed target program, SMOG2, is the most important upgrade for heavy-ion physics [15]. Depending on the beam energy, the centre-of-mass energies of the fixed-target collisions range from 40 to 115 GeV, between the SPS and RHIC energies. The forward acceptance of the LHCb geometry covers the middle and backward rapidity regions, providing access to high Bjorken-x region in the target nuclei. The installation of a gas storage cell upstream of the interaction point together with a new Gas Feed System for precise luminosity determination opens the door to many future measurements of great interest. The design of the SMOG2 storage cell is shown in the left panel of Fig. 7, the right panel shows a photo of the installed storage cell inside the LHCb detector together with the vertex detector VELO. With the new storage cell, more gas species such as H_2, D_2, N_2, O_2. Kr and Xe can be injected in addition to He, Ne and Ar. A well-defined interaction region of beam-gas collisions allows the possibility to record beam-gas and beam-beam collisions simultaneously without affecting the performance in the collider mode. The gas target areal density can be increased by up to 100 times, leading to higher luminosity for fixed-target collisions.

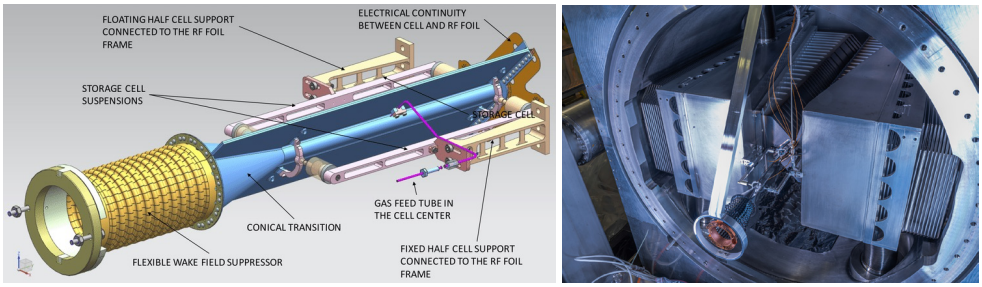

Figure 7. Left: design of the SMOG2 storage cell. Right: installed SMOG2 storage cell together with the VELO detector.

4 Conclusion and outlook

LHCb has a rich heavy ion program with excellent detector performance and unique kinematic coverage. The high statistical *p*Pb datasets offer valuable opportunities to perform precision measurements, study rare probes and investigate small Bjorken-x physics. First results from the PbPb datasets also demonstrate the capabilities of LHCb in studying nuclear effects in different systems. With the current upgrade, significantly increased statistics of *p*Pb and PbPb data samples in Run3 will allow for more precision measurements and open the possibilities for many new analyses. The upgrade will also unlock PbPb collisions up to mid-central events, enabling QGP studies with the LHCb detector. SMOG2 will bring the current fixed-target system to a new level with high statistics without detector saturation in unexplored energy and kinematic regions.

References

[1] A.A. Alves Jr. et al. (LHCb collaboration), JINST **3**, S08005 (2008)
[2] A. Kusina, J.P. Lansberg, I. Schienbein, H.S. Shao, Phys. Rev. Lett. **121**, 052004 (2018)
[3] A. Kusina, F. Lyonnet, D. Clark, E. Godat, T. Jezo, K. Kovarik, F. Olness, I. Schienbein, J. Yu, Eur. Phys. J. C **77**, 488 (2017), 1610.02925
[4] K.J. Eskola, P. Paakkinen, H. Paukkunen, C.A. Salgado, Eur. Phys. J. C **77**, 163 (2017), 1612.05741
[5] R. Aaij et al. (LHCb collaboration) (2021), in preparation
[6] I. Helenius, K.J. Eskola, H. Paukkunen, Journal of High Energy Physics **2014** (2014)
[7] T. Lappi, H. Mäntysaari, Phys. Rev. D **88**, 114020 (2013)
[8] Z.B. Kang, I. Vitev, E. Wang, H. Xing, C. Zhang, Physics Letters B **740**, 23 (2015)
[9] R. Aaij et al. (LHCb collaboration), Phys. Rev. **C103**, 064905 (2021), 2103.07349
[10] R. Aaij et al. (LHCb collaboration), JHEP **10**, 115 (2013), 1307.4285
[11] R. Aaij et al. (LHCb collaboration) (2020), in preparation
[12] W. Zha, S.R. Klein, R. Ma, L. Ruan, T. Todoroki, Z. Tang, Z. Xu, C. Yang, Q. Yang, S. Yang, Phys. Rev. C **97**, 044910 (2018)
[13] W. Zha, L. Ruan, Z. Tang, Z. Xu, S. Yang, Phys. Rev. C **99**, 061901 (2019)
[14] *Framework TDR for the LHCb Upgrade: Technical Design Report* (2012)
[15] *LHCb SMOG Upgrade* (2019)